Validation and application of caged Z-DEVD-aminoluciferin bioluminescence for assessment of apoptosis of wild type and TLR2-deficient mice after ischemic stroke

Josić Dominović, P.; Dobrivojević Radmilović, M.; Srakočić, S.; Mišerić, I.; Škokić, S.; Gajović, Srećko

Source / Izvornik: **Journal of Photochemistry and Photobiology B: Biology, 2024, 253**

Journal article, Published version
Rad u časopisu, Objavljena verzija rada (izdavačev PDF)

https://doi.org/10.1016/j.jphotobiol.2024.112871

Permanent link / Trajna poveznica: https://urn.nsk.hr/urn:nbn:hr:105:271637

Journal of Photochemistry & Photobiology, B: Biology 253 (2024) 112871

Contents lists available at ScienceDirect

Journal of Photochemistry & Photobiology, B: Biology

journal homepage: www.elsevier.com/locate/jphotobiol

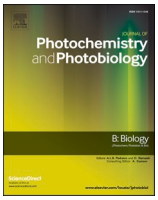

Validation and application of caged *Z*-DEVD-aminoluciferin bioluminescence for assessment of apoptosis of wild type and TLR2-deficient mice after ischemic stroke

P. Josić Dominović [a], M. Dobrivojević Radmilović [a], S. Srakočić [a], I. Mišerić [a], S. Škokić [a], S. Gajović [a,*]

[a] *University of Zagreb School of Medicine, BIMIS – Biomedical Research Center Šalata, and Croatian Institute for Brain Research, Zagreb, Croatia*

ARTICLE INFO

Keywords:
Toll-like receptor
Apoptosis
Bioluminescence
Caged luciferin
Ischemic stroke

ABSTRACT

Programmed cell death or apoptosis is a critically important mechanism of tissue remodeling and regulates conditions such as cancer, neurodegeneration or stroke. The aim of this research article was to assess the caged *Z*-DEVD-aminoluciferin substrate for *in vivo* monitoring of apoptosis after ischemic stroke in TLR2-deficient mice and their TLR2-expressing counterparts. Postischemic inflammation is a significant contributor to ischemic injury development and apoptosis, and it is modified by the TLR2 receptor. Caged *Z*-DEVD-aminoluciferin is made available for bioluminescence enzymatic reaction by cleavage with activated caspase-3, and therefore it is assumed to be capable of reporting and measuring apoptosis.

Apoptosis was investigated for 28 days after stroke in mice which ubiquitously expressed the firefly luciferase transgene. Middle cerebral artery occlusion was performed to achieve ischemic injury, which was followed with magnetic resonance imaging. The scope of apoptosis was determined by bioluminescence with caged *Z*-DEVD-aminoluciferin, immunofluorescence with activated caspase-3, flow cytometry with annexin-V and TUNEL assay.

The linearity of *Z*-DEVD-aminoluciferin substrate dose effect was shown in the murine brain. Z-DEVD-aminoluciferin was validated as a good tool for monitoring apoptosis following adequate adjustment. By utilizing bioluminescence of *Z*-DEVD-aminoluciferin after ischemic stroke it was shown that TLR2-deficient mice had lower post-stroke apoptosis than TLR2-expressing wild type mice. In conclusion, *Z*-DEVD-aminoluciferin could be a valuable tool for apoptosis measurement in living mice.

1. Introduction

Bioluminescence is a phenomenon of visible light emission in living organisms, inherently present in some marine animals, insects, and bacteria [1]. Visible light is emitted as a product of a biochemical reaction in which the luciferase enzyme oxidizes its substrate luciferin in the presence of ATP, oxygen, and magnesium [2]. Bioluminescence is adapted for the laboratory applications and recently used for imaging of small animals *in vivo*. The advantage of this approach is its non-invasiveness and the availability of various sensing probes. *In vivo* bioluminescence imaging is a remarkable method for monitoring of various cellular processes and physiological conditions in the living animals, their dynamics, and changes over time. Moreover, imaging living animals without noticeable side-effects, and the statistical advantage of longitudinally following the same animals during the whole experimental protocol represent significant ethical improvements.

The most used firefly luciferase (Fluc) comes from the North American firefly *Photinus pyralis* and utilizes the D-luciferin substrate. Other common luciferases originate from sea pansy *Renilla reniformis* (RLuc) and the copepod *Gaussia priceps* (GLuc) and they utilize coelenterazine as a substrate [3]. Modification of available substrates provides a source of sensors for observation and measurement of specific cellular and metabolic events. Among them, caged luciferins are initially non-reactive (caged) and subsequently chemically modified to be reactive (released from the cage). The luciferins with distinctive functional

Abbreviations: MRI, magnetic resonance imaging; BLI, Bioluminescence imaging; Luc, luciferase; TUNEL, terminal deoxynucleotidyl transferase (TdT); NeuN, neuronal nuclear protein.

* Corresponding author at: University of Zagreb School of Medicine, BIMIS – Biomedical Research Center Šalata, Šalata 4, HR-10000 Zagreb, Croatia.
E-mail address: srecko.gajovic@hiim.hr (S. Gajović).

https://doi.org/10.1016/j.jphotobiol.2024.112871
Received 9 November 2023; Received in revised form 6 February 2024; Accepted 20 February 2024
Available online 21 February 2024

groups combine additional chemical reactivity along with light-producing reaction. The modification of 6′-hydroxyl (amino) group of D-luciferin inhibits recognition by luciferase, therefore prohibiting the bioluminescent reaction and signal emission [4]. When analyte-reactive triggers are added there, luminescence can occur only after their cleavage with specific biological molecules (analytes). Such modifications of luciferin allow monitoring and characterization of processes of interest with molecular, spatial, and temporal specificity [5].

The subject of this study was caged *Z*-DEVD-aminoluciferin, which could be "released from the cage" only by active caspases-3 and -7, and subsequently available for luciferase-driven bioluminescence reaction [4]. The intensity of light signal emitted from the investigated system is assumed to be proportional to the level of caspase-3/7 - dependent apoptosis in the system [6]. The examples of applications of *Z*-DEVD-aminoluciferin include monitoring treatment-induced apoptosis in xenograft cancer models; *e.g.* in colon cancer treated with camptothecin, glioblastoma with temozolomide, and breast and ovarian cancers with docetaxel [6,7]. Our group applied *Z*-DEVD-aminoluciferin to assess the influence of altered innate immunity on apoptosis and brain repair after ischemic lesion in a mouse model with Gap43 promoter-driven luciferase expression [8].

The aim of this study was to validate *Z*-DEVD-aminoluciferin bioluminescence in the mouse brain using animals with ubiquitous luciferase expression. In the next step, we wanted to monitor apoptosis after ischemic brain lesion and relate it to the modified neuroinflammation in the TLR2-deficient mouse model.

TLR2 binds endogenous damage-associated molecular patterns (DAMPs) released after ischemic brain lesion. Subsequently, the activated TLR2 triggers the intracellular proinflammatory signaling pathways in local microglia [9]. Post-stroke inflammation influences the resulting damage and repair processes, also involving pro- and anti-apoptotic signaling [10–13]. After ligand binding, TLR2 initiates apoptosis through multiple molecular pathways, including the MyD88- and JNK-AP-1-dependent pathways [14,15]. However, TLR2's pro-apoptotic and anti-apoptotic activity are both present and their relationship is still elusive [14,16–18].

Using caged *Z*-DEVD-aminoluciferin bioluminescence imaging allowed us to longitudinally follow mice for 28 days after brain ischemic lesion, and to compare TLR2-deficient mice with ubiquitous luciferase expression (CAG-luc-Tlr2$^{-/-}$) and their wild type counterparts (CAG-luc-Tlr2$^{WT/WT}$). The extent of apoptosis determined by imaging was subsequently verified by immunofluorescence and flow cytometry, and the corresponding ischemic injury by *in vivo* magnetic resonance imaging and neurological scoring. Bioluminescence of growing doses of caged *Z*-DEVD-aminoluciferin substrate showed linearity in the brain. Caged Z-DEVD-aminoluciferin was found to be an adequate tool for monitoring apoptosis *in vivo* following necessary adjustment methods.

2. Materials and Methods

2.1. Animals

All animal procedures were assessed and approved by the Ethics Committee of the University of Zagreb School of Medicine, and by the Ministry of Agriculture Republic of Croatia. They were in accordance with the Ethical Codex of the Croatian Society for Laboratory Animal Science and with the EU Directive 2010/63/EU on the protection of animals used for scientific purposes. All experiments were performed on 12–16 weeks old male mice in accordance with the ARRIVE guidelines [19]. The animals were housed in the same environment; in a single room with temperature (22 ± 2 °C) and humidity control, in individually ventilated cages (Tecniplast Emerald ERGO, Italy) under 12/12 h light/dark cycles. Water and food were given *ad libitum*.

For the purpose of this study, a new mouse line C57BL/6-Tyr$^{c\text{-}Brd}$ -Tg(CAG-luc-GFP)^{Chco}-Tlr2$^{tm1Kir/Gaj}$ (depicted later in the text as CAG-luc-Tlr2$^{-/-}$) was created. This was a *Tlr2*-knockout line kept homozygous on albino background, which expressed firefly luciferase under the control of the ubiquitous CAG promoter. To create this line, C57BL/6-Tyr$^{c\text{-}Brd}$-Tlr2$^{tm1Kir/Gaj}$ mice (*Tlr2*-knockout) were mated with C57BL/6-Tyr$^{c\text{-}Brd}$-Tg(CAG-luc-GFP)$^{Chco/Gaj}$. In this study, the CAG-luc-Tlr2$^{-/-}$ mice were compared to their wild type (Tlr2$^{WT/WT}$) counterparts C57BL/6-Tyr$^{c\text{-}Brd}$ -Tg(CAG-luc-GFP)$^{Chco/Gaj}$ (depicted later in the text as CAG-luc-Tlr2$^{WT/WT}$). Included in the results are 65 CAG-luc-Tlr2$^{-/-}$, 59 CAG-luc-Tlr2$^{WT/WT}$ and 7 albino (C57BL/6-Tyr$^{c\text{-}Brd/Gaj}$) mice not carrying *luc* transgene. The genotypes of all animals were confirmed with PCR.

2.2. Transient Middle Cerebral Artery Occlusion

To induce a focal ischemic lesion of the brain, transient occlusion of the left middle cerebral artery (MCAO) was performed for 30 min by the Koizumi method [20]. The mice were anesthetized with 5% isoflurane gas (Isoflurane, Abbott, UK) kept at 2% for anesthesia maintenance. A silicon rubber-coated 6–0 monofilament (Doccol Corporation, Sharon, MA, USA) was introduced through the common carotid artery and advanced through the internal carotid artery, until the middle cerebral artery became occluded. The monofilament was removed after 30 min, allowing reperfusion [20]. After surgery, mice were kept in cages warmed on heated steel plates for the next 24 h. They were treated with i.p. injections of buprenorphine (0.05 mg/kg) for analgesia once a day for 3 days after surgery. Furthermore, they received i.p. injections of saline with 30% glucose (dosage 0.2 mL) for 3 days to prevent dehydration and weight loss. Until 7 days after surgery, food was softened to allow easier chewing. The animals were monitored for signs of humane endpoint until the end of the experiment. All investigators were blinded to all individual animals' experimental group allocations, ischemic lesion status or results of any performed measurements until the end of the experimental protocol.

2.3. Neurological Deficit Scoring

A modified neurological deficit scoring protocol was used, with the maximum number of points being 39 [20]. Higher scores corresponded to more severe neurological deficits caused by ischemic damage. The deficit exam consisted of a set of motor tests (muscle status, gait disturbances and spontaneous activity), sensory tests (tactile and proprioceptive), reflex tests and animal appearance. The animal weight was also followed and scored separately. The tests were performed at least twice before the experiment to get the animals acquainted with the protocol, and subsequently 7 days before and on days 2, 4, 7, 14 and 28 after MCAO.

2.4. Magnetic Resonance Imaging (MRI)

Magnetic resonance imaging (MRI) was performed on a 7 T system (BioSpec 70/20 USR with Paravision 6.1.1. software version, Bruker Biospin, Germany) in a Tx/Rx configuration, using an 86 mm transmit volume coil (MT0381, Bruker Biospin, Germany) for transmitting (Tx) and a 2-element mouse brain surface receive coil (MT0042, Bruker Biospin, Germany) for receiving (Rx). Mice were placed in an induction chamber and received 4% isoflurane anesthesia in a 70%/30% N2/O2 gas mixture. During imaging, anesthesia was maintained with 1–1.5% isoflurane. After initial anesthesia, mice were placed and secured inside a water-heated mouse bed in a prone position (Bruker, Germany). Their respiration rate was monitored with an optical probe (Medres, Germany) and kept in the range of 80–100 breaths/min. Body temperature was monitored using an MR-compatible rectal temperature probe (Medres, Germany) and maintained at 37 ± 0.5 °C by controlling the temperature of the water-heated bed and an additional body cover. Animals were imaged 7 days prior to MCAO (to establish the baseline), and on days 2, 7, 14, and 28 after MCAO. The scan protocol consisted of preparatory and main scans. A low-resolution multi slice localizer was run as a preparatory scan, while main scans included the T2-weighted

anatomical high-resolution scan in the coronal plane using a RARE sequence (time of echo/time of repetition TE/TR = 33/3000 ms, matrix size 160 × 100; field of view (FOV) 16 × 10 mm^2; slice thickness 0.4 mm; interslice distance 0.1 mm; number of slices 25) and the T2-map sequential protocol using a MSME sequence (TE/TR = 7.5/3150 ms; matrix size 128 × 80; FOV 16 × 10 mm^2; slice thickness 0,4 mm; interslice distance 0.1 mm; number of slices 25), from which T2 maps were calculated using the Paravision 6.1.1. software built-in post-processing macros. MRI exclusion criteria were applied during the first post-MCAO imaging session and consisted of unapparent lesion and hemorrhagic bleeding or hemorrhagic conversion of the ischemic lesion. Until day 7 after MCAO, the ischemic lesion was defined as a hyperintense area within the brain tissue in the T2 map modality. Due to edema loss in the later stages, at days 14 and 28 after MCAO, the direct measurement of lesion was impossible and was substituted with indirect measurement of lost tissue, which has previously been correlated with edema size at day 2 after stroke [20]. The tissue loss was calculated by subtracting the ipsilateral hemisphere volume at time point from the ipsilateral hemisphere volume at baseline. T2 scans were used to delineate the hemispheres in individual brain sections on all time points. T2 maps of the same brains were used to delineate the hyperintense areas of vasogenic edema on days 2 and 7. All delineations were done manually using the ImageJ 1.51n software (Wayne Rasband, National Institutes of Health USA). The corresponding volumes were calculated as the surface of all traced areas multiplied by the sum of section thicknesses and intersection distance.

2.5. In Vivo Bioluminescence Imaging (BLI)

In experiments aimed to determine the optimal dose of *Z*-DEVD-aminoluciferin (commercially available as VivoGlo™ Caspase-3/7 Substrate, Z-DEVD-Aminoluciferin, sodium salt, Promega, Madison, Wisconsin, USA), albino and CAG-luc-$Tlr2^{-/-}$ mice were anesthetized with 2% isoflurane in 100% oxygen in an induction chamber and placed in the heated light-tight imaging chamber of the IVIS Spectrum *In Vivo* Imaging System (PerkinElmer, Waltham, MA, USA) with constant inhalation anesthesia at 1.5 L/min and imaged before substrate injection to obtain background measurements. Subsequently, the mice were injected intraperitoneally with either *Z*-DEVD-aminoluciferin or D-luciferin in doses of 0.01, 0.1, 1, 10 and 100 mg/kg. A series of images was taken with open filter binning set to "high", field of view 25.2 × 25.2 cm, f/stop "1", with automatic exposure time every 2 min, repeated for approximately 95 min.

For *ex vivo* imaging, mice intraperitoneally received 10 mg/kg *Z*-DEVD-aminoluciferin (concentration 0.5 mg/mL in phosphate buffered saline, PBS) and their brains were isolated 15 min later. The isolated brains were imaged with open filter binning set to "high", field of view 6.6 × 6.6 cm, f/stop "1" and automatic exposure time every 2 min, repeated for approximately 26 min.

In the experiments dealing with animals with MCAO-induced ischemic brain lesion, measurements were performed on CAG-luc-$Tlr2^{-/-}$ and CAG-luc-$Tlr2^{WT/WT}$ strains with 10 mg/kg *Z*-DEVD-aminoluciferin (concentration 0.5 mg/mL PBS) and 1 mg/kg D-luciferin (concentration 0.15 mg/mL PBS). Background signal measurements were performed first. Subsequently, mice were injected intraperitoneally with the corresponding substrate, and a series of images was taken with open filter binning set to "high", field of view 25.2 × 25.2 cm, f/stop "1" and automatic exposure time every 2 min for approximately 56 min.

Total photon flux was measured in an ellipsoid region of interest encompassing the entire brain (*ex vivo*) or the skull surface directly above the brain (*in vivo*). The measurements were conducted using the Living Image 4.3 acquisition and imaging software (PerkinElmer, Waltham, MA, USA).

2.6. Immunofluorescence and TUNEL Assay

Mice were first transcardially perfused with phosphate buffered saline (PBS, pH 7.4, Kemika, Zagreb, Croatia), followed with 4% paraformaldehyde (PFA, Biognost, Zagreb, Croatia). The brains were subsequently isolated, prepared for histology, frozen, and stored at −80 °C in Tissue Tek medium (O.C.T. Compound, Sakura, USA). Brains were collected from healthy animals (4 CAG-luc-$Tlr2^{WT/WT}$ and 3 CAG-luc-$Tlr2^{-/-}$ animals) and from animals on days 7 and 28 after stroke induction. Data from 9 animals from each strain was analyzed for day 7, and from 4 animals for day 28. Frozen brains were carefully cut into 35 μm thick slices on a cryocut (Leica, Wetzlar, Germany) and mounted onto Superfrost Plus microscopic slides (Adhesion Microscope Slides, Epredia, USA). The following primary antibodies were used in cell death analysis: rabbit anti-cleaved caspase-3 primary antibody (1:100, #9661, Cell Signaling) and rat anti-NeuN (1:500, ab279297, Abcam). To visualize the stroke outline on immunofluorescence images, chicken anti-GFAP primary antibody (1:500, Abcam/ab4674) was used. The following secondary antibodies were utilized: Alexa Fluor 546 secondary antibody (donkey anti-rabbit, 1:500, A10040, Thermo Fisher Scientific), Alexa Fluor 488 secondary antibody (donkey anti-rat, 1:500, A-21208, Thermo Fisher Scientific) and Alexa Fluor 488 secondary antibody (goat anti-chicken, 1:500, A-11039, Thermo Fisher Scientific). All slices were stained with DAPI (10 mM, abcam, USA).

TUNEL assay was performed using the *In Situ* Cell Death Detection Kit, Fluorescein (Roche, Zurich, Switzerland). Frozen sections mounted on glass slides were prepared for the assay according to manufacturer's instructions. Briefly, after preparing the sections, 50 μL of TUNEL reaction mixture was added onto each slice. The slides were incubated in a humidified chamber at 37 °C for 60 min. Immediately after staining, the brain slices were observed under a confocal microscope.

The brain slices were observed under a confocal microscope (Olympus FV3000, Central Valley, PA, USA). Regions of interest were placed in the ipsilateral lesioned cortex (also referred to as cortex 1), perilesional cortex (also referred to as cortex 2) and lesioned striatum, as well as in corresponding contralateral areas. Immunofluorescence analysis was performed using the ImageJ 1.51n software (Wayne Rasband, National Institutes of Health USA). The captured signal of anti-cleaved caspase-3 and TUNEL assay was expressed as raw integrated density (RawIntDen) over region of interest surface area. Anti-NeuN signal was expressed as the number of anti-NeuN-positive cells over region of interest surface area and adjusted to the corresponding measurement in healthy brains.

2.7. Flow Cytometry

Mice were perfused with PBS and their brains were prepared for immunostaining following a protocol using accutase for enzymatic tissue digestion and a Percoll gradient for myelin removal [21]. The commercially available Apoptosis Kit with Alexa Fluor® 488 annexin-V and PI for Flow Cytometry (Invitrogen, V13245, Carlsbad, USA) was used to differentiate between apoptotic cells (positive for annexin-V), necrotic cells (positive for annexin-V and PI) and vital cells (negative for both). Flow cytometry was performed on the Attune® Acoustic Focusing Cytometer (Thermo Fisher Scientific, Waltham, USA).

2.8. Statistical Analysis and Visualizations

Statistical analysis was conducted in the GraphPad Prism Version 9.4.0 program GraphPad Software, San Diego, California, SAD). Normality of data distribution was assessed with statistical tests D'Agostino & Pearson and Shapiro-Wilk. Outlier analysis was performed by the ROUT method. Consequently, the discovered outliers were removed from measurements. After outlier analysis, mixed-effect ANOVA with Šidák post-hoc test was conducted for BLI, MRI, and neurological scoring results. For immunofluorescence, TUNEL and flow cytometry analyses,

non-parametric Mann-Whitney *U* test was used.

To visualize molecules of D-luciferin and *Z*-DEVD-aminoluciferin, the freely available program MolView was used.

3. Results

3.1. Application of Z-DEVD-Aminoluciferin for In Vivo Imaging of Apoptosis after Ischemic Brain Lesion

3.1.1. The Optimal Dose of Z-DEVD-Aminoluciferin Was Determined for Bioluminescence Imaging of Apoptosis in Ubiquitously Luciferase-Expressing Mice In Vivo

To determine the optimal dose of *Z*-DEVD-aminoluciferin, mice with ubiquitously expressed luciferase were imaged. The imaging was performed by series of doses (0.01, 0.1, 1, 10 and 100 mg/kg) of both *Z*-DEVD-aminoluciferin and D-luciferin (molecular forms of these luciferins are given in Fig. 1 (A, B)). The signal produced by growing doses of both substrates showed satisfactory linearity (Fig. 1 (C, D)). D-luciferin signal was higher than *Z*-DEVD-aminoluciferin for each dose ($P < 0.001$). Imaging with 100 mg/kg of D-luciferin resulted in signal oversaturation and could therefore not be quantified. For further experiments, to ensure optimal saturation of signal, the dose of 10 mg/kg of *Z*-DEVD-aminoluciferin was chosen over the 1 mg/kg dose.

3.1.2. The Transportation of Z-DEVD-Aminoluciferin across the Blood-Brain Barrier Was Validated Ex Vivo

Prior to using *Z*-DEVD-aminoluciferin to monitor apoptosis in brains of live animals, we tested whether the substrate was transported across the blood-brain barrier. Since ischemic damage influences the permeability of the blood brain barrier, the measuring was done at baseline on days 2 and 7 after stroke (3 animals at each time point). The imaging of Z-DEVD-aminoluciferin bioluminescence in isolated brains confirmed its transport into the brains of both the CAG-luc-Tlr2$^{WT/WT}$ and CAG-luc-Tlr2$^{-/-}$ mouse strains (Fig. 2 (A)). The signal was lateralized after the ischemic lesion. Comparing individual bioluminescence intensities for each brain revealed a trend of higher signals in CAG-luc-Tlr2$^{WT/WT}$ mice compared to CAG-luc-Tlr2$^{-/-}$ mice (Fig. 2 (B)).

3.1.3. In Vivo Bioluminescence Imaging of Apoptosis after Ischemic Stroke with Z-DEVD-Aminoluciferin Revealed Higher Signal in CAG-Luc-Tlr2$^{WT/WT}$ than CAG-Luc-Tlr2$^{-/-}$ Mice

The Z-DEVD-aminoluciferin substrate was employed to monitor the scope of apoptosis before and on days 2, 4, 7, 14 and 28 after ischemic stroke in living mice (Fig. 3 (A)). Bioluminescent signal was expressed as total flux (photon/s). Absolute total flux measurements revealed significantly higher bioluminescence signal ($P < 0.001$) in CAG-luc-Tlr2$^{WT/WT}$ than CAG-luc-Tlr2$^{-/-}$ mice during the entire experimental period (Fig. 3 (B)). Furthermore, the signal dynamics slightly differed between the strains. CAG-luc-Tlr2$^{WT/WT}$ mice had a higher bioluminescence signal at baseline ($P = 0.006$) and on days 2 ($P = 0.004$), 4 ($P < 0.001$) and 7 ($P = 0.026$) post-stroke.

3.1.4. In Vivo Bioluminescence Imaging with Free D-Luciferin Revealed Higher Signal in CAG-Luc-Tlr2$^{WT/WT}$ than CAG-Luc-Tlr2$^{-/-}$ Mice

Strain-specific blood-brain barrier permeability was investigated using D-luciferin based BLI imaging. To achieve this, we performed bioluminescence imaging with free D-luciferin substrate before and for 7 days after stroke (Fig. 3 (C)). The results revealed a significantly higher ($P = 0.027$) bioluminescent signal of free D-luciferin in CAG-luc-Tlr2$^{WT/WT}$ mice compared to CAG-luc-Tlr2$^{-/-}$ mice at baseline measurement (Fig. 3 (C)), indicating the existence of a confounding factor on luciferin bioavailability in the brain.

3.2. Normalization of Bioluminescence Signal to Minimize the Confounding Effects and Allow Comparisons between the Strains

3.2.1. TLR2 Deficiency Did Not Significantly Affect Ischemic Lesion Volumes in the Tested Strains

To be able to relate the bioluminescence signal to the ischemic brain lesion size we employed *in vivo* magnetic resonance imaging (MRI). MRI was applied at several time points before and during 28 days after stroke (Fig. 4 (A)). Stroke size was expressed as lesion volume during the acute

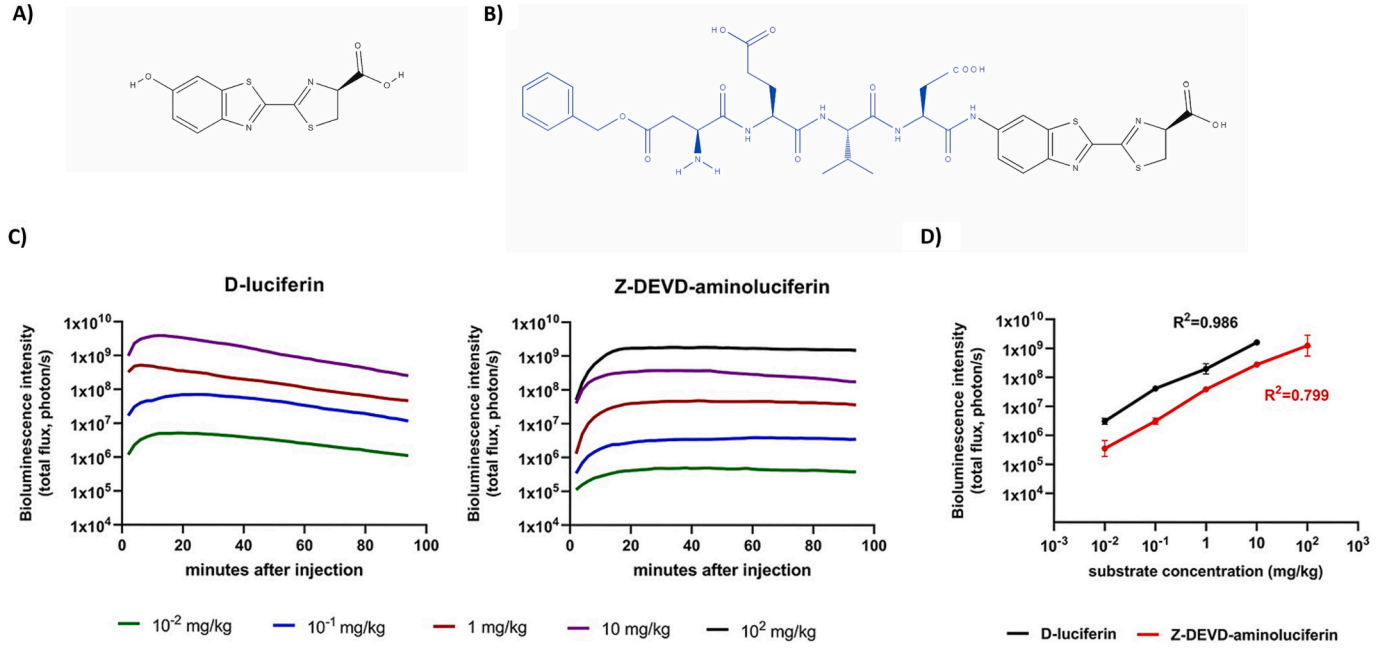

Fig. 1. A) D-luciferin molecule. B) *Z*-DEVD-aminoluciferin molecule. The "cage", DEVD tetrapeptide, is denoted in blue. C) Bioluminescence induced by ascending doses of D-luciferin (left) and *Z*-DEVD-aminoluciferin (right). D) Dose-response curve of bioluminescence intensities for D-luciferin and Z-DEVD-luciferin. Signal produced by growing doses of both substrates showed linearity ($R^2 = 0.986$ for D-luciferin and $R^2 = 0.799$ for *Z*-DEVD-aminoluciferin). Bioluminescence was quantified as total flux (photon/s) and the data were expressed as mean ± SD. The control animals without luciferin expression yielded no significant signal and therefore were not shown in the graphs. (For interpretation of the references to colour in this figure legend, the reader is referred to the web version of this article.)

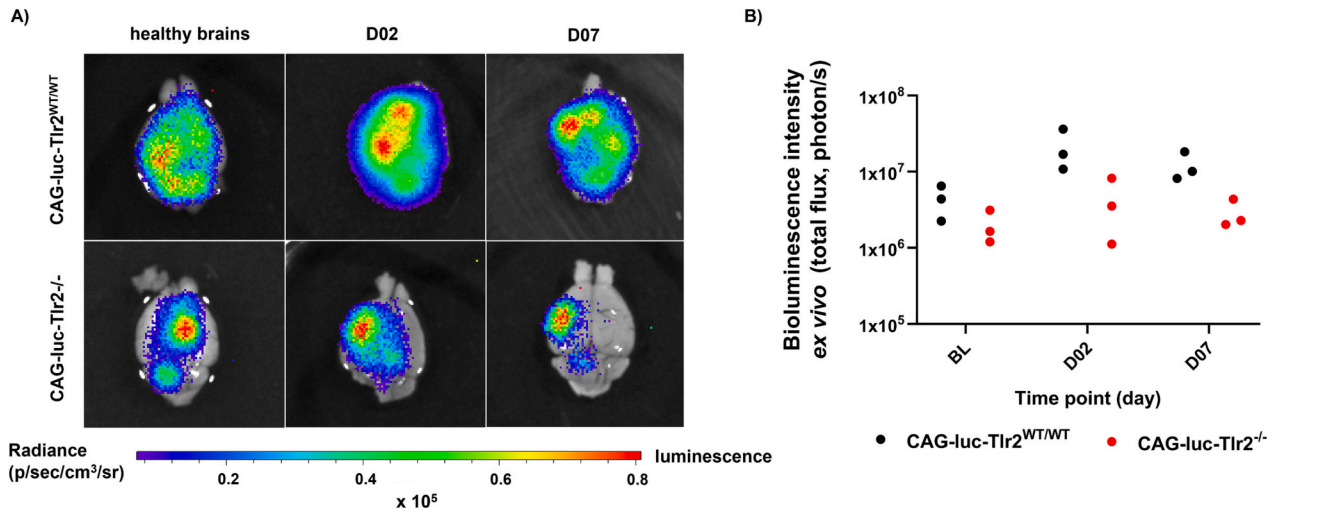

Fig. 2. A) *Ex vivo* imaging confirms the passage of *Z*-DEVD-aminoluciferin through the blood-brain barrier and its metabolism in the brain. B) Plot of Z-DEVD-aminoluciferin bioluminescence intensities in isolated brains of healthy mice (BL) and mice 2 and 7 days after stroke. BL – baseline.

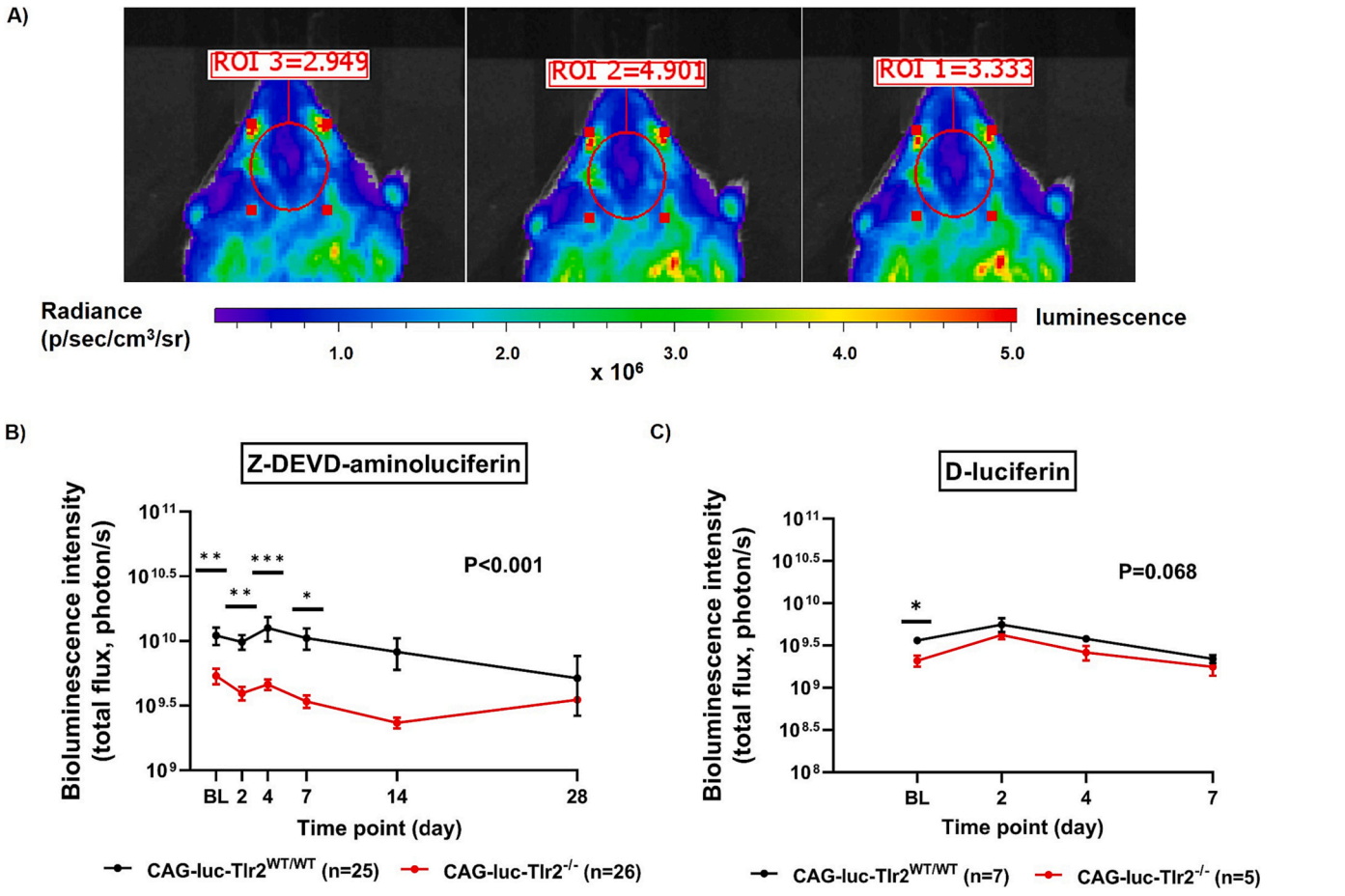

Fig. 3. A) Sequential images after *Z*-DEVD-aminoluciferin injection with delineated regions of interest. B) Absolute Z-DEVD-aminoluciferin bioluminescence at baseline and on 28 days after stroke expressed as total flux (photos/s). CAG-luc-Tlr2$^{WT/WT}$ mice have significantly higher signal of caged Z-DEVD-aminoluciferin at baseline ($P = 0.006$), on days 2 ($P = 0.004$), 4 ($P < 0.001$) and 7 ($P = 0.026$), as well as during the entire experimental period ($P < 0.001$). C) Absolute D-luciferin bioluminescence before (baseline, BL) and on 7 days post-stroke, expressed as total flux (photos/s). At baseline, CAG-luc-Tlr2$^{WT/WT}$ mice have significantly higher ($P = 0.028$) bioluminescent signal of D-luciferin than CAG-luc-Tlr2$^{-/-}$ mice. Values indicate mean ± SEM, *$P < 0.05$. BL – baseline.

phase (mm^3), and as the volume of lost tissue calculated by subtracting the ipsilateral hemisphere volume at time point from the ipsilateral hemisphere volume at baseline during the chronic period (Fig. 4 (B)). The lesion size did not differ between the analyzed mouse strains during the experimental period.

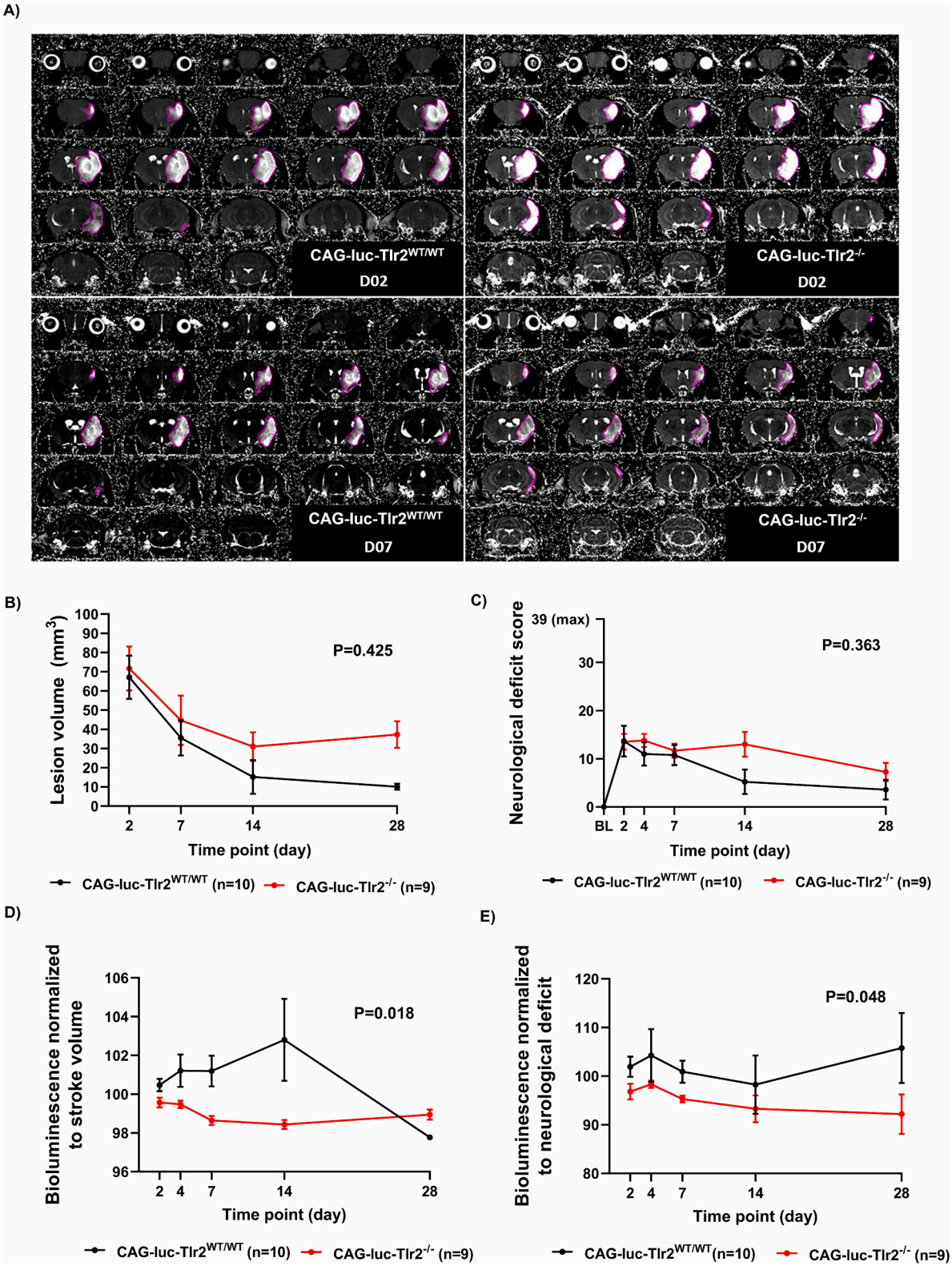

Fig. 4. A) T2 map images of lesions for CAG-luc-Tlr2$^{WT/WT}$ and CAG-luc-Tlr2$^{-/-}$ mice on days 2 and 7 after stroke. B) Stroke volumes (mm^3) during 28 days after stroke did not differ between CAG-luc-Tlr2$^{WT/WT}$ and CAG-luc-Tlr2$^{-/-}$ mice ($P = 0.425$). C) Neurological deficit scores did not differ between CAG-luc-Tlr2$^{WT/WT}$ and CAG-luc-Tlr2$^{-/-}$ mice ($P = 0.363$). D) *Z*-DEVD-aminoluciferin bioluminescence intensities adjusted according to the formula (1 + [(BLI$_{tp}$/BLI$_{bl}$)-1] / ST$_{tp}$) x 100) showed a significantly higher bioluminescence signal in CAG-luc-Tlr2$^{WT/WT}$ than CAG-luc-Tlr2$^{-/-}$ mice during the 28 days after stroke ($P = 0.018$). E) Z-DEVD-aminoluciferin bioluminescence intensities adjusted according to the formula (1 + [(BLI$_{tp}$/BLI$_{bl}$)-1] / NS$_{tp}$) x 100) were significantly different between the strains, with CAG-luc-Tlr2$^{WT/WT}$ mice having higher signal than CAG-luc-Tlr2$^{-/-}$ mice ($P = 0.048$). Values indicate mean ± SEM, *$P < 0.05$. BL – baseline, BLI – bioluminescence imaging, tp– time point, bl – baseline, ST – stroke volume, NS – neurological score.

3.2.2. TLR2 Deficiency Had no Effect on Neurological Deficiency after Stroke

Neurological deficit scoring was not different between the strains (Fig. 4 (C)). However, body weight monitoring revealed a higher body weight in CAG-luc-Tlr2$^{-/-}$ mice on day 2 after stroke ($P = 0.016$), as well as across the entire experimental period ($P = 0.004$) (data not shown).

3.2.3. The Signal of Caged Z-DEVD-Aminoluciferin Bioluminescence Normalized to the Baseline Bioluminescence and Lesion Size at the Day of Measurement Was Higher in CAG-Luc-Tlr2$^{WT/WT}$ than CAG-Luc-Tlr2$^{-/-}$ Mice

To minimize the confounding effect of different substrate bioavailability between the strains, we performed an adjustment of *Z*-DEVD-aminoluciferin bioluminescence signal at every time point after stroke to bioluminescence signal at baseline and stroke volume at the day of measurement, according to the formula $(1 + [(BLI_{tp}/BLI_{bl})\text{-}1] / ST_{tp}) \times 100$) (BLI – bioluminescence imaging, tp– time point, bl – baseline, ST – stroke). To achieve this, we only included the animals that survived at least until day 7. Since we did not perform MRI on day 4 after stroke, the approximate lesion volume on day 4 was calculated as an arithmetic mean of lesion volumes on days 2 and 7. This minimization of the confounding effect allowed further comparison of bioluminescence intensities between the strains and revealed a significant difference in *Z*-DEVD-aminoluciferin signal intensity between the strains, with CAG-luc-Tlr2$^{WT/WT}$ mice having higher bioluminescence signal than CAG-luc-Tlr2$^{-/-}$ animals ($P = 0.018$) during the experimental period (Fig. 4 (D)). Furthermore, Z-DEVD-aminoluciferin bioluminescence intensities were significantly higher during the whole acute and subacute period than on day 28, corresponding to stroke resolution processes.

3.2.4. The Signal of Caged Z-DEVD-Aminoluciferin Bioluminescence Normalized to the Baseline Bioluminescence and Neurological Deficiency Score at the Day of Measurement Was Higher in CAG-Luc-Tlr2$^{WT/WT}$ than CAG-Luc-Tlr2$^{-/-}$ Mice

The signal of caged Z-DEVD-aminoluciferin at every time point after stroke was further adjusted to bioluminescence signal at baseline and neurological deficiency score at the day of measurement, according to the formula $(1 + [(BLI_{tp}/BLI_{bl})\text{-}1] / NS_{tp}) \times 100$) (BLI – bioluminescence imaging, tp– time point, bl – baseline, NS – neurological score). This calculation revealed a functional correlation between bioluminescence and functional deficit, as well as a significant difference in *Z*-DEVD-aminoluciferin signal intensity between the strains, with CAG-luc-Tlr2$^{WT/WT}$ mice having higher bioluminescence signal than CAG-luc-Tlr2$^{-/-}$ animals ($P = 0.048$) (Fig. 4 (E)).

3.3. Cell Death Analyses

3.3.1. Cleaved Caspase-3 Immunofluorescence in Ipsilateral Perilesional Cortex and Striatum Was Higher in CAG-Luc-Tlr2$^{WT/WT}$ than CAG-Luc-Tlr2$^{-/-}$ Mice

To validate the imaging results and to determine the extent of apoptosis in mouse brains after stroke, cryopreserved mouse brain slices were stained with anti-cleaved caspase-3 antibody on days 7 and 28 post-stroke (Fig. 5 (A, B)). Healthy animals from each strain were used as negative controls (equivalent to the status before the ischemic lesion). Anti-cleaved caspase-3 signal was calculated as raw integrated density (RawIntDen) per μm^2. No cleaved caspase-3 signal was detected in healthy (control) brains. On day 7, there was a pronounced signal of cleaved caspase-3 in the ipsilateral hemisphere of both strains. The Mann-Whitney *U* test confirmed a more significant signal of cleaved caspase-3 in ipsilateral perilesional cortex (cortex 2) of CAG-luc-Tlr2$^{WT/WT}$ than CAG-luc-Tlr2$^{-/-}$ mice on day 7 ($(P < 0.001)$, Fig. 5 (C)). Furthermore, CAG-luc-Tlr2$^{WT/WT}$ mice had significantly more caspase-3 than CAG-luc-Tlr2$^{-/-}$ mice in the ipsilateral striatum on day 7 ($P = 0.014$). The signal of caspase-3 significantly increased from baseline to day 7 in cortex 1 of CAG-luc-Tlr2$^{WT/WT}$ ($P = 0.004$) mice, as well as in cortex 1 of CAG-luc-Tlr2$^{-/-}$ ($P = 0.009$) animals. In the same region, caspase-3 signal significantly decreased from day 7 to day 28 in CAG-luc-Tlr2$^{WT/WT}$ ($P = 0.004$) and CAG-luc-Tlr2$^{-/-}$ ($P = 0.003$) animals. In cortex 2, caspase-3 signal significantly increased from baseline to day 7 in CAG-luc-Tlr2$^{WT/WT}$ ($P = 0.003$) and CAG-luc-Tlr2$^{-/-}$ ($P = 0.009$) animals, and significantly decreased between days 7 and 28 in CAG-luc-Tlr2$^{WT/WT}$ ($P = 0.003$) mice. The same dynamic was reflected in the ipsilateral striatum, where caspase-3 signal grew significantly from baseline to day 7 in CAG-luc-Tlr2$^{WT/WT}$ ($P = 0.003$) and CAG-luc-Tlr2$^{-/-}$ ($P = 0.018$) mice, and it significantly lowered on day 28 compared to day 7 in the CAG-luc-Tlr2$^{WT/WT}$ ($P = 0.011$) strain.

Cleaved caspase-3 signal was lower in contralateral hemisphere compared to ipsilateral hemisphere of both strains.

3.3.2. TUNEL Assay Showed no Differences in Post-Stroke Apoptosis between the Strains

The extent of cell death after ischemic stroke was further investigated with TUNEL assay on cryopreserved mouse brain slices before and on days 7 and 28 after stroke (Fig. 6 (A, B)). Healthy animals from each strain were used as negative controls. TUNEL signal was calculated as raw integrated density (RawIntDen) per μm^2. No TUNEL signal was detected in healthy (control) brains. On day 7, a widespread signal of TUNEL-positive cells was found in ipsilateral regions of interest in both strains (Fig. 6 (B)). In cortex 1 region of the ipsilateral hemisphere, TUNEL assay signal significantly increased between baseline and day 7 in CAG-luc-Tlr2$^{WT/WT}$ mice ($P = 0.006$), as well as in CAG-luc-Tlr2$^{-/-}$ mice ($P = 0.017$). TUNEL signal decreased between days 7 and 28 in the same region in CAG-luc-Tlr2$^{WT/WT}$ ($P = 0.042$) and CAG-luc-Tlr2$^{-/-}$ mice ($P = 0.006$). In cortex 2, TUNEL signal significantly increased from baseline to day 7 in CAG-luc-Tlr2$^{WT/WT}$ ($P = 0.006$) and CAG-luc-Tlr2$^{-/-}$ ($P = 0.017$) animals, and significantly decreased between days 7 and 28 in CAG-luc-Tlr2$^{WT/WT}$ ($P = 0.017$) mice. The same was recorded in the ipsilateral striatum, where TUNEL signal grew significantly from baseline to day 7 in CAG-luc-Tlr2$^{WT/WT}$ ($P = 0.003$) and CAG-luc-Tlr2$^{-/-}$ ($P = 0.017$) mice, and it significantly lowered on day 28 compared to day 7 in the CAG-luc-Tlr2$^{WT/WT}$ ($P = 0.011$) strain. However, there were no statistically significant differences in TUNEL assay signal between the genotypes (Fig. 6 (C)).

3.3.3. Loss of NeuN – Postive Neurons in Ipsilateral Perilesional Cortex Was Higher in CAG-Luc-Tlr2$^{WT/WT}$ than in CAG-Luc-Tlr2$^{-/-}$ Mice

To determine the extent of neuronal loss in mouse brains after stroke, cryopreserved mouse brain slices were stained with anti-NeuN antibody on days 7 and 28 post-stroke (Fig. 7 (A)). Healthy animals from each strain were used as negative controls. The number of anti-NeuN-positive cells is expressed per μm^2, normalized to the same measurement in healthy brains. Neuronal nuclei number analysis showed that CAG-luc-Tlr2$^{WT/WT}$ mice had significantly fewer neurons in ipsilateral perilesional cortex (cortex 2) on day 7 after stroke than CAG-luc-Tlr2$^{-/-}$ mice ($P = 0.003$), (Fig. 7 (B, C)). These results are complementary to increased apoptosis in perilesional cortex of CAG-luc-Tlr2$^{WT/WT}$ mice on day 7 after stroke. Furthermore, in CAG-luc-Tlr2$^{WT/WT}$ mice the number of neurons significantly increased from day 7 to day 28 in ipsilateral cortex 1 ($P = 0.028$).

3.3.4. Flow Cytometry with Annexin-V and Propidium Iodide Associated TLR2 Deficiency with More Pronounced Post-Stroke Brain Necrosis

Reactivity of flipped phosphatidylserine with annexin-V was another hallmark of apoptotic cells considered. The flow cytometry was performed with annexin-V as an apoptosis marker, and propidium iodide, which could only bind DNA of dead cells (Fig. 8 (A)). There was no significant difference in the percentage of annexin-V-positive cells in whole brains on day 7 after stroke between the strains (Fig. 8 (B)). However, the CAG-luc-Tlr2$^{-/-}$ sample contained more of annexin-V and propidium iodide double positive cells than the CAG-luc-Tlr2$^{WT/WT}$

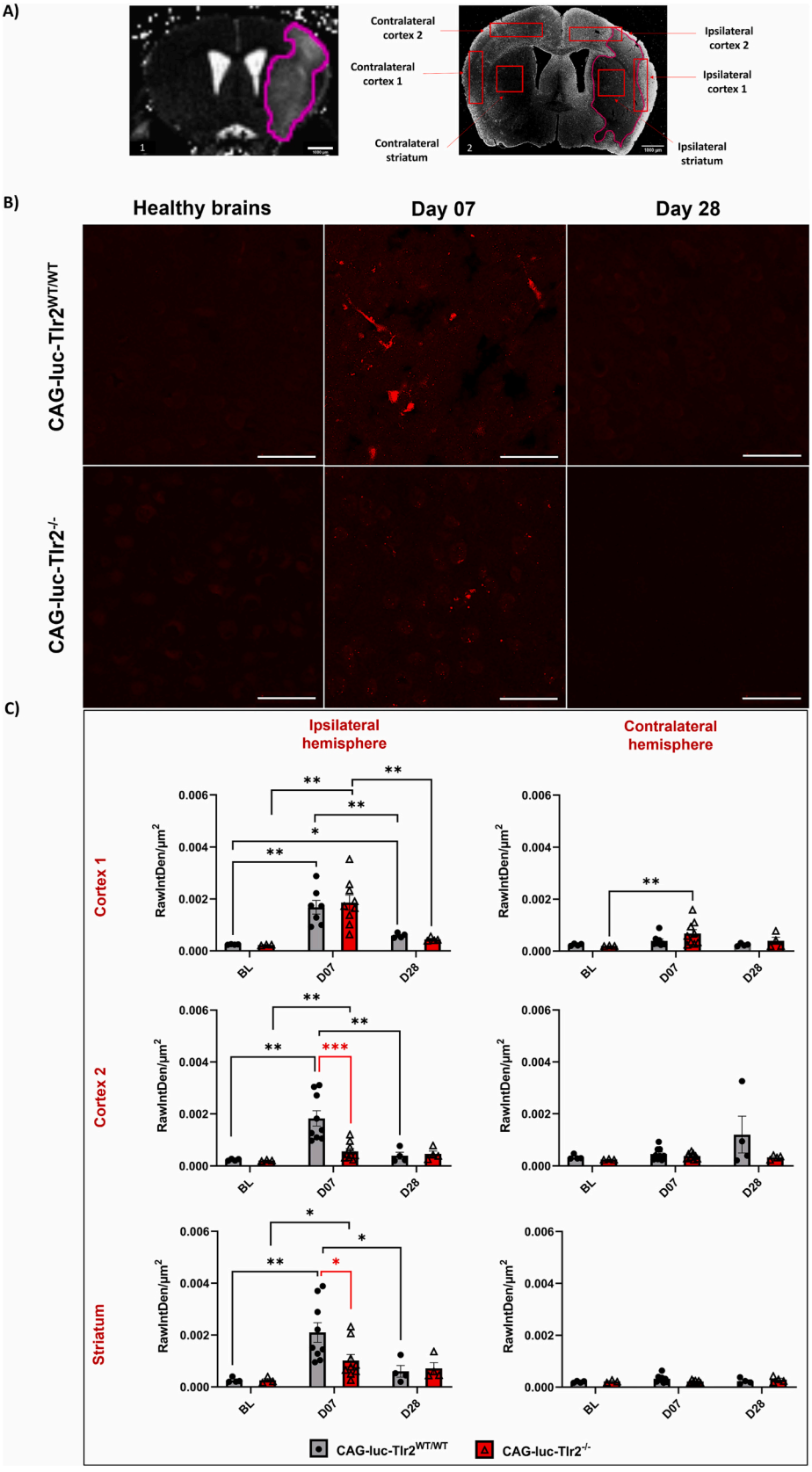

(caption on next page)

Fig. 5. A) MRI-generated image of stroke on day 7 in the mouse brain (image A1, left), and the corresponding lesion location in an immunofluorescence-obtained image of the same brain (image A2, right). Representative regions of interest are marked with red rectangles in cortex 1, cortex 2 and striatum of MCAO experimental groups. B) Immunofluorescence with anti-cleaved caspase-3 antibody in ipsilateral cortex 2 in healthy brains and on days 7 and 28 after stroke. The caspase signal is most pronounced on day 7. C) Expression of cleaved caspase-3 antibody in all regions of interest in the ipsilateral and contralateral hemispheres on days 7 and 28 after stroke. On day 7, CAG-luc-Tlr2$^{WT/WT}$ mice have significantly more cleaved caspase-3 compared to CAG-luc-Tlr2$^{-/-}$ mice in the perilesional cortex (cortex 2) ($P < 0.001$) and striatum ($P = 0.014$) of the ipsilateral hemisphere (significant comparisons between strains indicated in red). Values indicate mean ± SEM, $^{*}P < 0.05$. Scale bar: 50 μm. (For interpretation of the references to colour in this figure legend, the reader is referred to the web version of this article.)

sample, meaning that more necrotic cells were present ($P = 0.005$) (Fig. 8 (C)). Both measurements were shown as the percentage of stained cells on day 7 compared to healthy brains.

4. Discussion

One of the main results of this study is that caged *Z*-DEVD-aminoluciferin *in vivo* bioluminescence is suitable for measurement of apoptosis in the mouse brain. We successfully confirmed the linearity of the bioluminescence signal and showed bioluminescence in the mouse brain. Since the molecular weight of *Z*-DEVD-aminoluciferin is roughly three times larger than that of D-luciferin, it was questioned whether it had the ability to cross the blood-brain barrier. Following intraperitoneal injection of *Z*-DEVD-aminoluciferin, the substrate crossed the blood-brain barrier, and its bioluminescence was specifically achieved in the subsequently isolated brains. Furthermore, in these brains the strongest bioluminescent signal was lateralized to the affected hemisphere after ischemic lesion. However, due to extensive swelling and edema formation during the acute phase of the stroke, the effects of the ischemic injury also reached the right brain hemisphere. Severe mechanical injury exerted by the swelling on the contralateral hemisphere leads to tissue and cell death, as do numerous biochemical and metabolic post-stroke processes. Therefore, in addition to the bioluminescent signal in the ipsilateral hemisphere, Z-DEVD-aminoluciferin imaging detected caspase-3 activation and apoptotic cell death in the contralateral hemisphere.

Caged Z-DEVD-aminoluciferin has previously been extensively described in cancer research, cell and tissue transplantation, immunology, and stroke [6–8,22]. However, a dose-response and validation study had not been conducted on brains of mice with ubiquitous expression of luciferase until now.

The specifically challenging task was to validate whether Z-DEVD-aminoluciferin bioluminescence corresponds to apoptosis in the brain after ischemia, and if it can be used to compare two mouse models, wild type (CAG-luc-Tlr2$^{WT/WT}$) *versus* mice with modified neuroinflammation (CAG-luc-Tlr2$^{-/-}$). The initial bioluminescence measurement before ischemia already showed a significant difference between the strains. To verify if these differences arose due to the different bioavailability of the substrate because of differences in blood-brain permeability, we compared native bioluminescence between the strains using free D-luciferin. There was a significant difference between the two mouse strains after measurement of bioluminescence in brains of naïve animals, which supported possible differences in blood-brain barrier between the strains. Subsequently, to remove the influence of different blood-brain barrier permeabilities between the strains, we analyzed post-ischemic lesion results according to the baseline measurements (animals before the lesion).

Moreover, we decided to capitalize on the additional imaging modality (MRI) performed on the same animal, and we additionally adjusted the bioluminescence signal at a certain time point according to the brain lesion size obtained with MRI (to compensate for variable tissue loss in the analyzed brains). This adjustment allowed to reveal an increase in bioluminescence signal during the acute and subacute phases of ischemic lesion development in wild type animals and their higher bioluminescence compared to Tlr2$^{-/-}$ animals. We would recommend the strategy of analyzing bioluminescence based on baseline values and additional imaging modalities in any experiments performed on mouse brains. Similar approaches are regularly used in our group [8,18].

The subsequent question to be answered was if significant differences between the two strains reflect post-ischemic apoptosis, which was validated by immunohistochemistry and flow cytometry. The more precise immunofluorescence methods confirmed higher apoptosis in the perilesional areas and striatum of wild type mice than those of Tlr2$^{-/-}$ mice. Flow cytometry with annexin-V was employed to further investigate post-stroke apoptosis. Caspase-3 is one of the upstream modulators of phosphatidylserine inversion, which is a hallmark of apoptotic cell death. However, phosphatidylserine inversion is not dependent on caspase-3 nor TLR2. Although wild type mice had more cleaved caspase-3, other caspases such as caspase-1, −8 and − 9 can influence phosphatidylserine exposure on cell surface and lead to apoptosis [23]. *Z*-DEVD-aminoluciferin imaging investigated only caspase-3/7-dependent apoptosis, and immunofluorescence with cleaved caspase-3 was utilized to validate those measurements. Therefore, flow cytometry with annexin-V revealed potential additional mechanisms of apoptosis in TLR2-deficient mice, which could not be investigated with the methods employed in this study.

The advantage of *in vivo* imaging modalities, including *Z*-DEVD-aminoluciferin, is their ability to visualize temporal brain changes after ischemia. The evolution of post-ischemic damage and subsequent repair involves a multitude of mechanisms, which makes this analysis very challenging [1324,25,26]. This challenge is particularly present in the analysis of post-mortem brains isolated at specific time points. We suggest that these challenges are in the background of different results obtained when comparing apoptosis between the strains [8,18,27]. Moreover, other mechanisms of cell death are involved. Flow cytometry with annexin-V and propidium iodide analysis showed significantly more necrosis in whole brains of Tlr2$^{-/-}$ than wild type mice on day 7 after stroke. The relationship between TLR2 deficiency and increased necrosis is yet to be elucidated. Perhaps the clinically most relevant parameters of ischemic injury are functional deterioration and recovery, and all of the complex celluar and molecular mechanisms in the brain are summarized and reflected in them. Although neurological score does not influence bioluminescence production, we further adjusted bioluminescence signal according to the neurological score, as it is in essence of all post-ischemic events, and it additionally confirmed higher caged *Z*-DEVD-aminoluciferin bioluminescence in wild type animals.

Bioluminescence imaging of the brain is highly influenced by the blood-brain barrier permeability to the large Z-DEVD-aminoluciferin, but also the smaller D-luciferin, whose signal was also significantly different between the strains at baseline. The role of TLR2 in apoptosis after stroke has been a debated question. The connection between TLR2 and apoptosis is well documented, with most studies reporting that blocking TLR2 *in vivo* protects against progression of ischemic injury and apoptosis [11,28,29]. After ligand binding, TLR2 initiates apoptosis through multiple molecular pathways, the most important one being the MyD88-dependent pathway. TLR2 signals through the MyD88 adapter protein, which binds FADD. FADD in turn activates caspase-8, leading to the cleavage and activation of caspase-3 [14]. TLR2 signaling has also been proven to trigger caspase-3-dependent apoptosis through the JNK-AP-1 pathway after mouse brain ischemia [15]. The opposite, protective role of TLR2 knock-out post stroke and subsequent lower apoptosis has been discussed as well [27]. Furthermore, the negative effect of TLR2 on blood-brain barrier integrity, which affects substrate bioavailability in the brain, has been extensively described in literature [30–32]. TLR2 is present on brain endothelial cells and disrupts proteins occludin and claudin during inflammation [32]. TLR2 also induces expression of

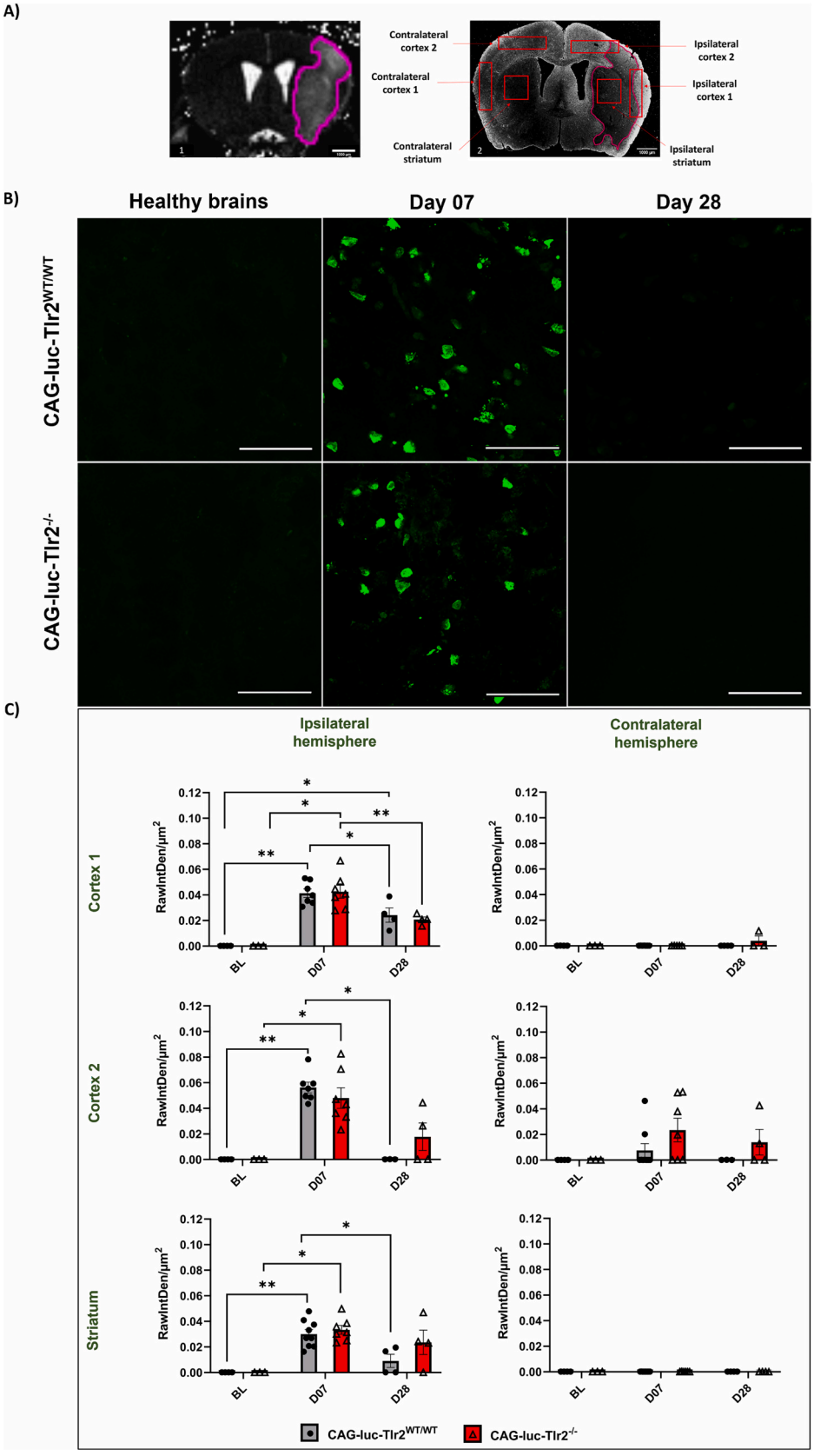

Fig. 6. A) MRI-generated image of stroke on day 7 in the mouse brain (image A1, left), and the corresponding lesion location in an immunofluorescence-obtained image of the same brain (image A2, right). Representative regions of interest are marked with red rectangles in cortex 1, cortex 2 and striatum of MCAO experimental groups. B) TUNEL assay in ipsilateral cortex 2 in healthy brains and on days 7 and 28 after stroke, with the highest signal present on day 7. C) There is no difference in the signal of TUNEL-positive cells between the strains for all regions of interest and during the experimental period. Values indicate mean ± SEM, $*P < 0.05$. Scale bar: 50 µm. (For interpretation of the references to colour in this figure legend, the reader is referred to the web version of this article.)

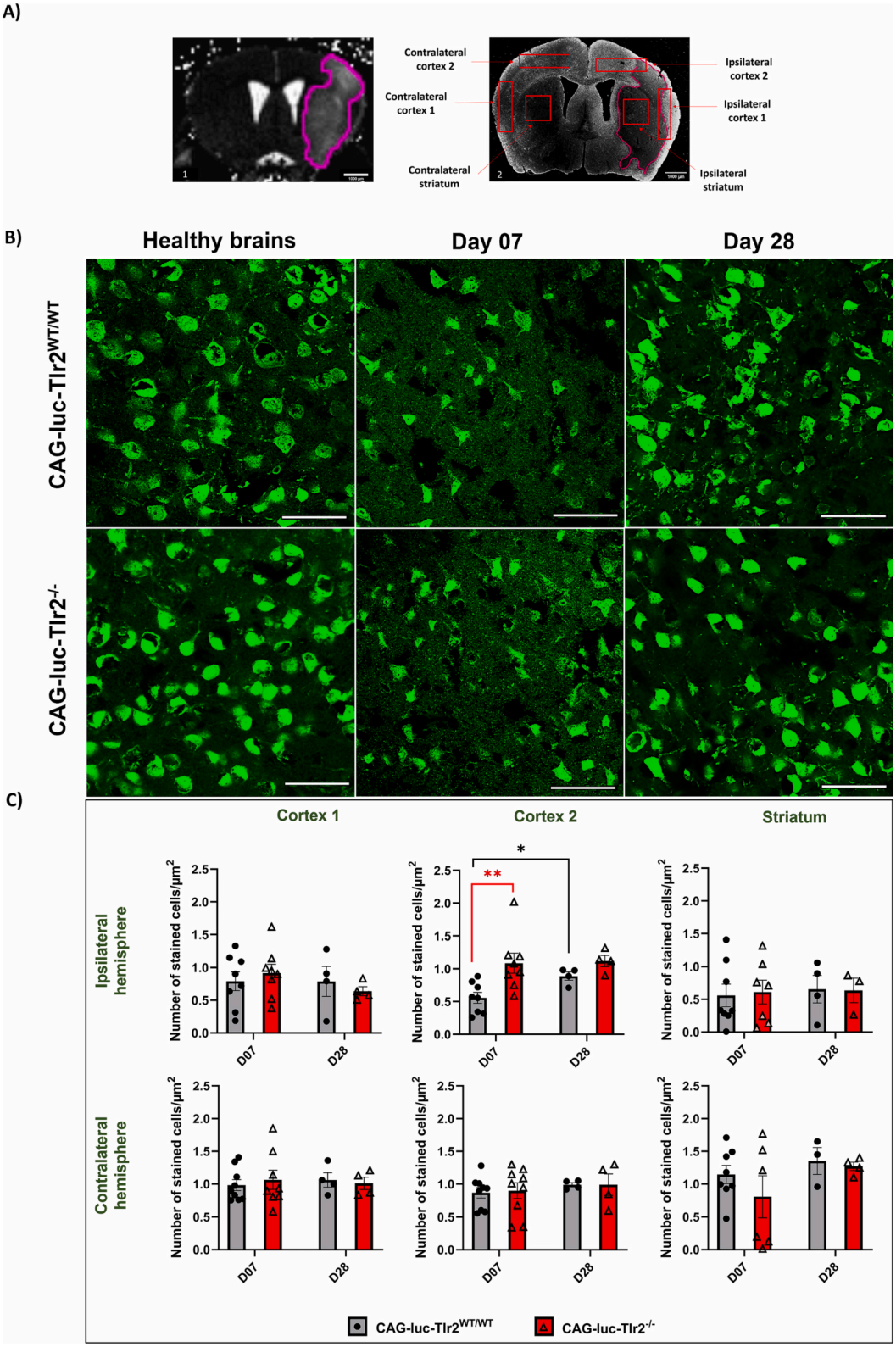

Fig. 7. A) MRI-generated image of stroke on day 7 in the mouse brain (image A1, left), and the corresponding lesion location in an immunofluorescence-obtained image of the same brain (image A2, right). Representative regions of interest are marked with red rectangles in cortex 1, cortex 2 and striatum of MCAO experimental groups. B) Immunofluorescence with anti-NeuN antibody in ipsilateral cortex 2 in healthy brains and on days 7 and 28 after stroke. After stroke, less neurons are found than in healthy brains. C) CAG-luc-Tlr2$^{WT/WT}$ mice have significantly fewer neurons than CAG-luc-Tlr2$^{-/-}$ animals in the perilesional cortex (cortex 2) of ipsilateral hemisphere on day 7 ($P = 0.003$) (significant comparisons between strains indicated in red). Neuronal numbers significantly increased in ipsilateral cortex 2 of CAG-luc-Tlr2$^{WT/WT}$ mice between days 7 and 28 (P = 0.028). Values indicate mean ± SEM, *$P < 0.05$. Scale bar: 50 µm. (For interpretation of the references to colour in this figure legend, the reader is referred to the web version of this article.)

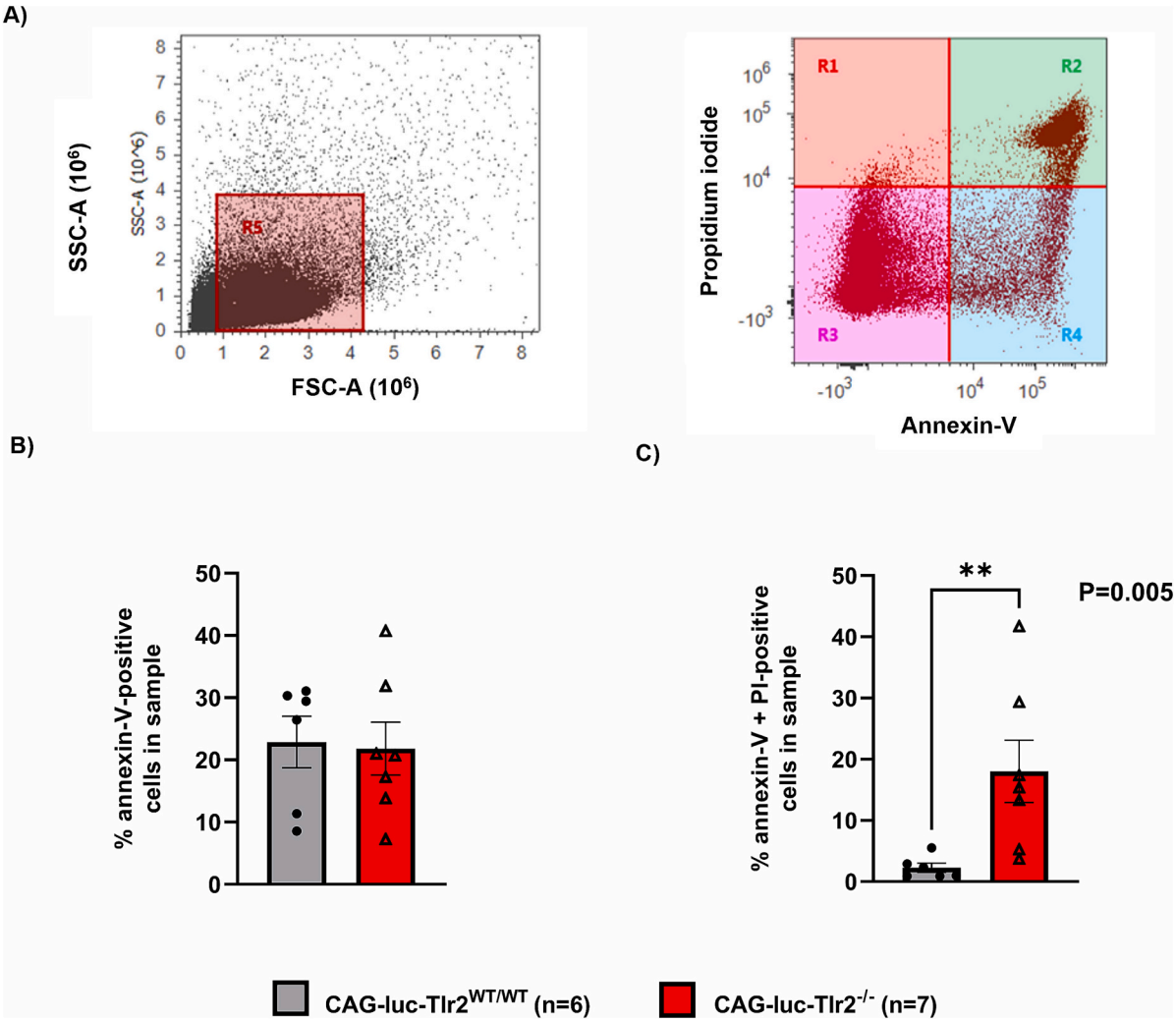

Fig. 8. A) Gating strategy for apoptotic cells using flow cytometry. The cells were first sorted based on their forward (FSC) and side (SSC) scatter (left), followed by separation annexin-V and propidium iodide (right). Healthy cells are found in R3 quadrant (annexin – V^- propidium $iodide^-$), apoptotic cells (annexin-V^+ propidium $iodide^-$) cells are found in the R4 quadrant, while the necrotic cells (annexin-V^+ propidium $iodide^+$) are found in the R2 quadrant. B) There was no difference in the percentage of annexin-V-positive cells in the whole brains between the strains on day 7 after stroke. C) CAG-luc- $Tlr2^{-/-}$ mice had significantly more ($P = 0.005$) both annexin-V- and propidium iodide-positive cells on day 7 after stroke than CAG-luc-$Tlr2^{WT/WT}$ mice, suggesting more pronounced necrosis. Values indicate mean ± SEM, $^*P < 0.05$.

matrix metalloproteinase-9, a matrix-degrading enzyme which breaks down neurovascular matrix and blood-brain barrier tight junctions [30]. Therefore, the significant difference in bioluminescence intensities between the strains could be a consequence of the combined effect of increased bioavailability of caged *Z*-DEVD-aminoluciferin and increased post-ischemic TLR2-dependent apoptosis, and subsequently, enhanced Z-DEVD-aminoluciferin signal, in wild type compared to $Tlr2^{-/-}$ mice.

The limitations of this study are common to all longitudinal stroke research, which in this case lasted 28 days. The animals suffered as a consequence of ischemia and some of them were lost during this period. The study would benefit from including more animals, however longitudinality is essential in ethical and sustainable small animal research. In conclusion, caged Z-DEVD-aminoluciferin was examined and assessed as a good tool for monitoring total apoptosis *in vivo*. The design of future experiments focusing on identifying and measuring apoptosis will depend on individual needs, which may call for combining *in vivo* with *ex vivo* experiments and molecular methods.

Funding

This study was supported by the Croatian Science Foundation project RepairStroke (IP-06-2016-1892), and by the European Union through the European Regional Development Fund, under Grant Agreement No. KK.01.1.1.07.0071, project "Sinergy of molecular markers and multimodal in vivo imaging during preclinical assessment of the consequences of the ischemic stroke (SineMozak)", and under Grant Agreement No. KK.01.1.1.04.0085, project "Genomic engineering and gene regulation in cell lines and model organisms by CRISPR/Cas9 technology – CasMouse".

CRediT authorship contribution statement

P. Josić Dominović: Conceptualization, Data curation, Formal analysis, Investigation, Methodology, Project Administration, Software, Supervision, Validation, Writing - original draft, Writing - review & editing. **M. Dobrivojević Radmilović:** Methodology, Resources, Supervision, Validation, Writing - review & editing. **S. Srakočić:** Investigation, Writing - review & editing. **I. Mišerić:** Investigation, Writing - review & editing. **S. Škokić:** Methodology, Project administration, Resources, Software, Supervision, Validation, Writing - review & editing. **S. Gajović:** Conceptualization, Funding acquisition, Methodology, Project administration, Resources, Software, Supervision, Validation,

Writing - original draft, Writing - review & editing.

Declaration of competing interest

None.

Data availability

On request to corresponding author.

Acknowledgments

In vivo imaging was done at core facility of the Laboratory for Regenerative Neuroscience – GlowLab, University of Zagreb School of Medicine. The work of doctoral students Paula Josić and Sanja Srakočić was fully supported by the "Young researchers' career development project – training of doctoral students" of the Croatian Science Foundation funded by the European Union from the European Social Fund.

References

[1] R.T. Sadikot, T.S. Blackwell, Bioluminescence imaging, Proc. Am. Thorac. Soc. 2 (6) (2005) 537–540.
[2] B.W. Rice, M.D. Cable, M.B. Nelson, In vivo imaging of light-emitting probes, J. Biomed. Optics. 6 (4) (2001) 432–440.
[3] J.W. Hastings, Chemistries and colors of bioluminescent reactions: a review, Gene. 173 (1 Spec) (1996) 5–11.
[4] J. Li, L. Chen, L. Du, M. Li, Cage the firefly luciferin! - a strategy for developing bioluminescent probes, Chem. Soc. Rev. 42 (2) (2013) 622–676.
[5] T.A. Su, K.J. Bruemmer, C.J. Chang, Caged luciferins for bioluminescent activity-based sensing, Curr. Opin. Biotechnol. 60 (2019) 198–204.
[6] M. Scabini, F. Stellari, P. Cappella, S. Rizzitano, G. Texido, E. Pesenti, In vivo imaging of early stage apoptosis by measuring real-time caspase-3/7 activation, Apoptosis. 16 (2) (2011) 198–207.
[7] J. Hickson, S. Ackler, D. Klaubert, J. Bouska, P. Ellis, K. Koster, et al., Noninvasive molecular imaging of apoptosis in vivo using a modified firefly luciferase substrate, Z-DEVD-aminoluciferin, Cell Death Differ. 17 (6) (2010) 1003–1010.
[8] D. Gorup, S. Škokić, J. Križ, S. Gajović, Tlr2 deficiency is associated with enhanced elements of neuronal repair and caspase 3 activation following brain ischemia, Sci. Rep. 9 (1) (2019) 2821.
[9] Y. Wang, P. Ge, Y. Zhu, TLR2 and TLR4 in the brain injury caused by cerebral ischemia and reperfusion, Mediat. Inflamm. 2013 (124614) (2013).
[10] F. Arslan, B. Keogh, P. McGuirk, A.E. Parker, TLR2 and TLR4 in ischemia reperfusion injury, Mediat. Inflamm. (2010) 704202.
[11] G. Ziegler, D. Harhausen, C. Schepers, O. Hoffmann, C. Röhr, V. Prinz, et al., TLR2 has a detrimental role in mouse transient focal cerebral ischemia, Biochem. Biophys. Res. Commun. 3 (359) (2007) 574–579.
[12] J.H. Hayward, S.J. Lee, A decade of research on TLR2 discovering its pivotal role in glial activation and Neuroinflammation in neurodegenerative diseases, Exper. Neurobiol. 23 (2) (2014) 138–147.
[13] A.B. Uzdensky, Apoptosis regulation in the penumbra after ischemic stroke: expression of pro- and antiapoptotic proteins, Apoptosis. 24 (9–10) (2019) 687–702.
[14] A.O. Aliprantis, R.B. Yang, D.S. Weiss, P. Godowski, A. Zychlinsky, The apoptotic signaling pathway activated by toll-like receptor-2, EMBO J. 19 (13) (2000) 3325–3336.
[15] S.C. Tang, T.V. Arumugam, X. Xu, A. Cheng, M.R. Mughal, D.G. Jo, J.D. Lathia, D. A. Siler, S. Chigurupati, X. Ouyang, T. Magnus, S. Camandola, M.P. Mattson, Pivotal role for neuronal toll-like receptors in ischemic brain injury and functional deficits, Proc. Natl. Acad. Sci. USA 104 (34) (2007) 13798–13803.
[16] H. Izadi, A.T. Motameni, T.C. Bates, E.R. Olivera, V. Villar-Suarez, I. Joshi, et al., C-Jun N-terminal kinase 1 is required for toll-like receptor 1 gene expression in macrophages, Infect. Immun. 75 (10) (2007) 5027–5034.
[17] B. Salaun, P. Romero, S. Lebecque, Toll-like receptors' two-edged sword: when immunity meets apoptosis, Eur. J. Immunol. 37 (12) (2007) 3311–3318.
[18] D. Gorup, I. Bohaček, T. Miličević, R. Pochet, D. Mitrečić, J. Križ, S. Gajović, Increased expression and colocalization of GAP43 and CASP3 after brain ischemic lesion in mouse, Neurosci. Lett. 597 (2015) 176–182.
[19] C. Kilkenny, W.J. Browne, I.C. Cuthill, M. Emerson, D.G. Altman, Improving bioscience research reporting: the ARRIVE guidelines for reporting animal research, PLoS Biol. 8 (6) (2010).
[20] Justić H, Barić A, Šimunić et al. Redefining the Koizumi model of mouse cerebral ischemia: a comparative longitudinal study of cerebral and retinal ischemia in the Koizumi and longa middle cerebral artery occlusion models. J. Cereb. Blood Flow Metab. 2022; 42(11): 2080–2094.
[21] S. Srakocic, P. Josic, S. Trifunovic, S. Gajovic, D. Grcevic, A. Glasnovic, Proposed practical protocol for flow cytometry analysis of microglia from the healthy adult mouse brain: systematic review and isolation methods' evaluation, Front. Cell. Neurosci. 16 (1017976) (2022).
[22] K. Hochgräfe, E.M. Mandelkow, Making the brain glow: in vivo bioluminescence imaging to study neurodegeneration 47 (2013) 868–882.
[23] S.B. Bratton, M. MacFarlane, K. Cain, G.M. Cohen, Protein complexes activate distinct caspase cascades in death receptor and stress-induced apoptosis, Exp. Cell Res. 256 (1) (2000) 27–33.
[24] RA Felberg, WS Burgin, JC Grotta, Neuroprotection and the ischemic cascade, CNS Spectrums 5 (3) (2000) 52–58.
[25] A Rosell, E Cuadrado, A Ortega-Aznar, M Hernández-Guillamon, EH Lo, J Montaner, MMP-9-positive neutrophil infiltration is associated to blood-brain barrier breakdown and basal lamina type IV collagen degradation during hemorrhagic transformation after human ischemic stroke, Stroke 39 (4) (2008) 1121–1126.
[26] MS Sekhon, PN Ainslie, DE Griesdale, Clinical pathophysiology of hypoxic ischemic brain injury after cardiac arrest: a "two-hit" model, Critical Care 21 (1) (2017) 90.
[27] I. Bohaček, P. Cordeau, M. Lalancette-Hébert, D. Gorup, Y.C. Weng, S. Gajović, J. Križ, Toll-like receptor 2 deficiency leads to delayed exacerbation of ischemic injury, J. Neuroinflammation 9 (2012) 191.
[28] G. Ziegler, D. Freyer, D. Harhausen, U. Khojasteh, W. Nietfeld, G. Trendelenburg, Blocking TLR2 in vivo protects against accumulation of inflammatory cells and neuronal injury in experimental stroke, J. Cereb. Blood Flow Metab. 31 (2) (2011) 757–766.
[29] S. Lehnardt, S. Lehmann, D. Kaul, K. Tschimmel, O. Hoffmann, S. Cho, et al., Toll-like receptor 2 mediates CNS injury in focal cerebral ischemia, J. Neuroimmunol. 190 (1–2) (2007) 28–33.
[30] H. Zhu, R. Dai, H. Fu, Q. Meng, MMP-9 upregulation is attenuated by the monoclonal TLR2 antagonist T2.5 after oxygen-glucose deprivation and Reoxygenation in rat brain microvascular endothelial cells, J. Stroke Cerebrovasc. Dis. 28 (1) (2019) 97–106.
[31] F. Takata, S. Nakagawa, J. Matsumoto, S. Dohgu, Blood-brain barrier dysfunction amplifies the development of Neuroinflammation: understanding of cellular events in brain microvascular endothelial cells for prevention and treatment of BBB dysfunction, Front. Cell. Neurosci. 13 (15) (2021).
[32] V. Rajeev, D.Y. Fann, Q.N. Dinh, H.A. Kim, T.M. De Silva, M.K.P. Lai, et al., Pathophysiology of blood brain barrier dysfunction during chronic cerebral hypoperfusion in vascular cognitive impairment, Theranostics 12 (4) (2022) 1639–1658.